

Gravity anomalies and disturbances in the oceanic crust around the Galápagos islands

Charles Hoots

Abstract

This report contains processing and interpretations of gravity anomalies in the region surrounding the Galápagos islands. Gravity measurements were taken at a recent cruise in the area. Using the recovered data, the Free-air, gravity disturbances, simple Bouguer, and complete Bouguer anomalies are processed then compared with their counterpart's subset from a global gravity reference model. Each anomaly and disturbance evaluated shows broad agreement with the global reference model. The free-air anomaly shows both features consistent with sea-floor topography superimposed on broader structure likely related to upwelling along the Cocos ridge and western GSC. Free-air disturbances from the geoid were compared with an isostatically compensated disturbance to highlight features that are explained by isostasy to understand the relative importance of flexure in this region. The simple and complete Bouguer anomalies show smoother and fine features consistent with lateral variations in density structure of the crust and mantle lithosphere, respectively. From the anomalies and disturbances evaluated, we show localized features consistent with the Galápagos hotspot and detailed mantle upwelling structures as larger negative anomalies along the Cocos ridge compared to the western Galápagos Spreading Center (GSC).

Introduction

The Galápagos Islands region represents a complex geodynamic setting shaped by the interaction between the Galápagos mantle plume and the nearby Cocos–Nazca spreading system. Volcanism within the archipelago is broadly organized into an eastward age-progressive trend consistent with the motion of the Nazca Plate over a relatively fixed hotspot source (Sinton et al., 1996; Harpp and Geist, 2018). To the north, the Galápagos Spreading Center (GSC) defines an active mid-ocean ridge that accommodates divergent motion between the Cocos and Nazca plates. This spreading center exhibits strong segmentation and geochemical variability, reflecting heterogeneous mantle melting and the influence of plume material migrating from the hotspot to the ridge axis (Ito & Bianco, 2014). Offset to the northwest of the projected apex of the GSC Gore is the Cocos–Nazca–Pacific triple junction, one of only three ridge–ridge–ridge (RRR) triple junctions on Earth (DeMets et al., 1990; Cronin, 1992). With complex and rare examples of intraplate volcanism and plate-boundary processes, the surrounding region offers strong constraints on the nature of plume–ridge interaction, upper mantle flow, and the distribution of magmatic and tectonic activity. These processes, which influence the thermal and compositional structure of the oceanic crust and underlying mantle lithosphere, have indirect influences on gravity observations (Zheng et al., 2023). More fundamentally, variations in gravity anomalies help to constrain the relative importance between isostasy and flexure as the oceanic lithosphere ages and thickens with increasing distance from the GSC (Kirby, 2019; Watts, 2001). This report highlights gravity anomalies and free-air disturbances that capture the integrated effects of these processes and others.

Data

The data consists of approximately 7,800 km of gravity measurements taken at an average 1-km spacing starting from Golfito, Costa Rica and traveling southwest to the Galápagos islands during the recovery cruise for the Iguana seismic (Hooft et al., 2023). Subsequent analysis of this experiment's multi-dimensional (seismic, bathymetry, and gravity) data set of high-quality measurements seek to understand by what mechanisms do mantle plume materials flow and disperse toward the GSC to the north and how might small-scale heterogeneities influence the plume's convective rheology as this occurs. Undoubtedly, readers of this report can help to answer these questions.

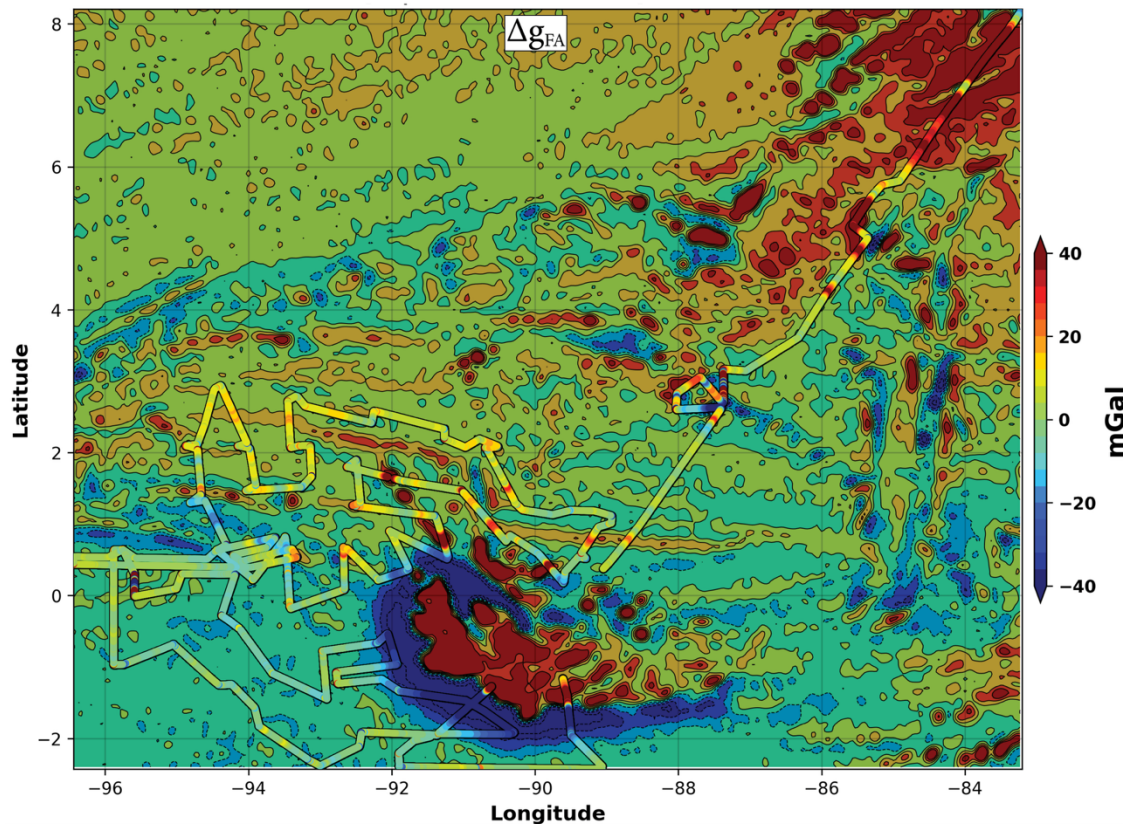


Figure 1. The Free-Air surface gravity anomaly from the Iguana recovery cruise. Embossed line is the free-air anomaly of the data collected during the Iguana recovery cruise. For comparison, the map background is the Free-Air surface gravity anomaly from the 2012 World Gravity Model (WGM2012; Bonvalot et. al., 2012). Both the map and Iguana cruise free-air anomaly data share an identical colormap where WGM2012 is slightly darker to make easy visual distinctions between the two. Free-air anomalies over the ocean show large sensitivity to seafloor topography superimposed on broader features such as mantle upwelling along the Cocos ridge.

The data used in my analysis begins with the free-air anomaly (**figure 1**), corrected for perturbation in the measured gravity due to the centrifugal acceleration experienced by the shipboard gravimeter as it moves relative to Earth's rotation (Eötvös, 1922). For a reasonable comparison with anomalies in this data, we utilize the 2012 World Gravity Model (WGM2012; Balmino & Bonvalot, 2016). WGM2012 consists of a high-resolution (2-minute) global gravity model for free-air and complete Bouguer anomalies as well as a Bouguer anomaly following an Airy isostatic compensation to a depth of 30km below the geoid. For correction terms that require the geoid height anomaly (see eq. 2), we use the EGM2008 (Pavlis, 2012) geoid anomaly geoid height (in meters) above the WGS84 (Lemoine et al., 1998) reference ellipsoid (**figure 2**). The geoid begins above the ellipsoid off the coast of South America where the Iguana recovery begins, dropping below within about 400km of the Galápagos islands.

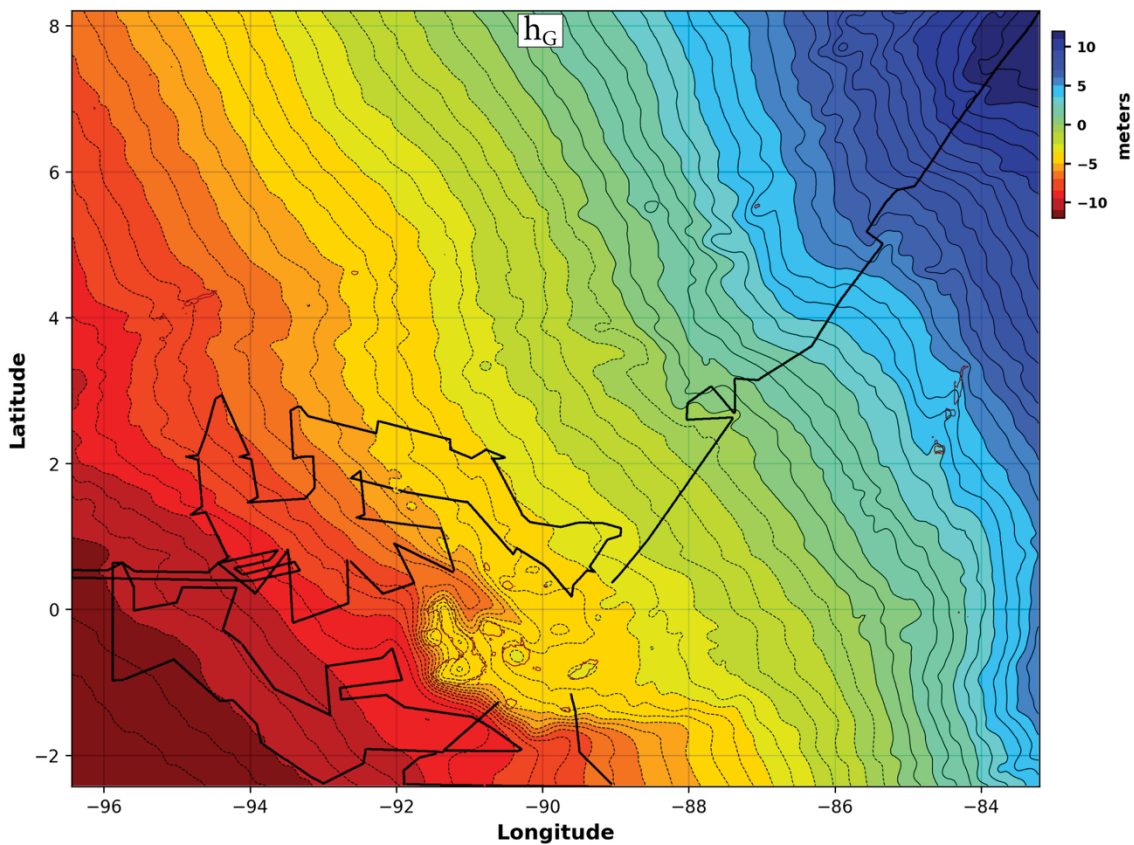


Figure 2. Geoid height anomaly (Pavlis et al., 2012) around the Galapagos islands. Shown on this map is height (h_G) of the geoid in meters above the reference ellipsoid (WGS84; NGA, 1984). The ship track for the Iguana recovery cruise is labeled with a black line.

Method

$$\Delta g_{FA} = g_{obs} - g_{FA} - g_0 \quad \text{eq. 1}$$

The free-air gravity anomaly (Δg_{FA} , *eq. 1*) represents the difference between the observed gravity (g_{obs}) and the normal gravity predicted on the reference ellipsoid (g_0) at the same horizontal location. It includes a correction (g_{FA}) for the elevation of the observation point, assuming a vacuum (appropriately named “free-air”), effectively modeling how

gravity would behave if continued downward from the observation to the ellipsoid. Of course when already at sea level, this correction is zero. However, even at sea level, differences between the geoid and the reference ellipsoid can introduce a bias into the anomaly. This bias is due to the free-air anomaly referencing the ellipsoid, while the observation is located on the geoid. The free-air gravity disturbance (δg_{FA} , eq. 2) corrects for this by accounting for the vertical separation between the two surfaces, the geoid height anomaly (h_g).

$$\delta g_{FA} = \Delta g_{FA} + h_g * 0.3086 \quad \text{eq. 2}$$

When the geoid lies above the ellipsoid (positive height anomaly), Δg_{FA} underestimates the true gravitational deviation due to comparing against a lower (weaker) reference. The free-air disturbance corrects this by adding back the gravitational effect of the vertical separation, making it larger than the free-air anomaly (Chapman and Bodine, 1979). Conversely, when the geoid is below the ellipsoid (negative height anomaly), Δg_{FA} overestimates the anomaly, and the disturbance reduces it accordingly. While the difference between a free-air anomaly and a free-air disturbance at sea level is typically never more than ~30 mGal (Hackney and Featherstone, 2003), the disturbance more accurately reflects mass deficits that cause lateral undulations in the geoid — such as first-order effects related to variations in the depth of the Moho or other major density contrasts.

If using the free-air anomaly in a Bouguer slab approximation for the moho depth or a more sophisticated spectral method such as the Parker-Oldenborg inversion (Parker, 1973; Oldenburg, 1974) the residual between Δg_{FA} and δg_{FA} can approximate the resulting discrepancy in their moho depth calculation given by δh_m ,

$$\delta h_m = \frac{\Delta g_{FA} - \delta g_{FA}}{2\pi\gamma\Delta\rho} \quad \text{eq. 3}$$

Where γ and $\Delta\rho$ are the gravitational constant and density contrast expected at the depth of the moho, respectively. Using the free-air anomaly from the recovery cruise, we also approximate the simple and complete Bouguer anomaly along the ship track for a reasonable comparison with WGM2012. The simple bouguer anomaly is made from the subtraction of the attraction for an infinitely wide slab and finite thickness from the free-air anomaly with the equation

$$\Delta g_{SB} = \Delta g_{FA} - 2\pi\gamma\rho_c h = \Delta g_{FA} - 0.1119 * 10^{-5}h \quad \text{eq. 4}$$

Where h is height above sea-level and the scalar constant ($2\pi\gamma\rho_c = 0.1119 * 10^{-5}$) is for a slab density of 2,670 kg/m³. This assumption systematically underestimated the Bouguer anomaly relative to a denser oceanic crust (~2,900 kg/m³). While this is a slab density consistent with continental crust despite the study region being exclusively oceanic crustal density, this density choice simplifies comparisons with WGM2012 and the eventual progression from a simple to a complete Bouguer anomaly. When using bathymetry for measurements at sea-level to produce the simple Bouguer anomaly, the definition of h

remains the same and h is taken as the negative of bathymetry. In effect, flipping the sign for slab correction at sea-level. This convention for the use of bathymetry in eq. 4 is standard, with my resulting anomalies being very consistent with prior studies in the region that show simple Bouguer anomalies (e.g. Barrera-Lopez et al., 2022). Using the infinite slab equation in the simple Bouguer anomaly essentially replaces the density of water with that of continental crust by not accounting for the topographic relief between sea-level and seafloor. The complete Bouguer anomaly (Δg_{CB} , eq. 6) is produced from a terrain correction term (eq. 5) subtracted from the simple Bouguer anomaly using LaFehr's method for a cylindrical approximation of the gravity contrast between the crust and underlying water column out to a radius of 1km,

$$g_t = \Delta\rho 2\pi\gamma[R - \sqrt{(R^2+z^2)+z}] \quad \text{eq. 5}$$

$$\Delta g_{CB} = \Delta g_{SB} - g_t \quad \text{eq. 6}$$

Where R is the radius of the water column cylinder (1km) and z is its height (bathymetric depth) and $\Delta\rho$ the density between the crust and water (1.67 kg/m^3). Since the measurements are taken at an average 1km spacing with a 2.3% average change in relief

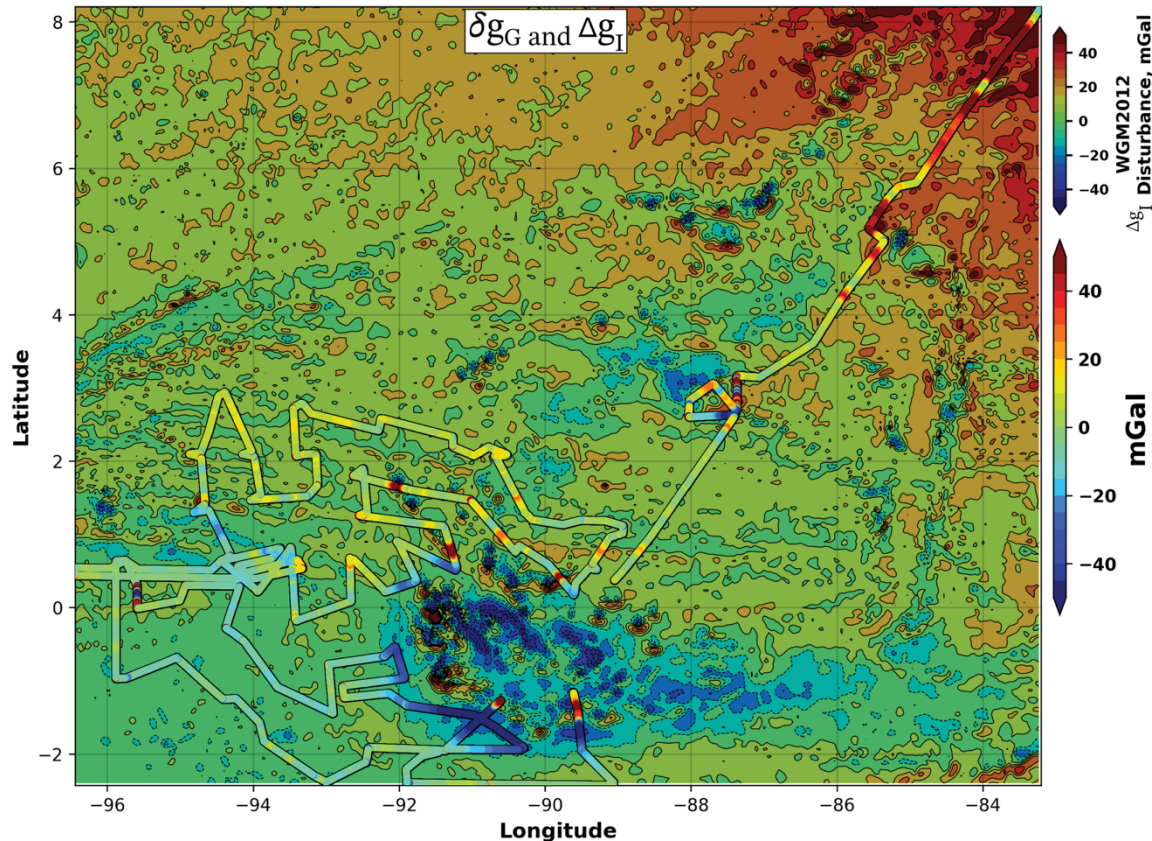


Figure 3. Gravity disturbance (δg_G) of the free-air surface anomaly between gravity on the ellipse and geoid. This represents the free-air anomaly that would be produced if the reference surface were the geoid instead of the reference ellipsoid. As a result, lateral variations in the disturbance are directly comparable with the geoid gravity anomaly. For comparison, the map background is a Bouguer anomaly isostatically compensated to a depth of 30km (Δg_I , Bonvalot et al., 2012).

between each, the integrated effect is a reasonably continuous profile beneath the ship for the correction term. While this is a likely fine method for correction at this scale of gravity observation, it does not capture long-wavelength terrain effects such as those used in the global terrain corrections in the WGM2012 model.

Results

The free-air gravity disturbance (δg_{FA} , eq. 2) is shown in figure 3. While not directly comparable with each other given their different processing steps, the underlying map in figure 3 is the WGM2012's gravity anomaly (Airy) isostatically compensated to a depth of 30km. With this in mind, we see finer features in the gravity disturbance along the ship path coincident with similar features in the isostatically compensated. For example, when compared with the free-air anomaly in figure 1, the positive anomaly along the Cocos spreading ridge is absent to slightly negative in the isostatic anomaly. The negative free-air disturbances (figure 3) also show finer lateral variations between the volcanic islands compared to the free-air anomalies (figure 2). Using eq. 3, figure 4 shows the correction to a moho depth approximation when using the free-air anomaly varying by about +/- 100m along the ship path from the continental coast out to the islands. This result is expected, as the difference between the free-air anomaly and disturbance is essentially just the geoid gravity anomaly (see eq. 2). Figure 5 shows simple and complete Bouguer anomalies for the recovered data on the Iguana recovery cruise in comparison with their counterparts in

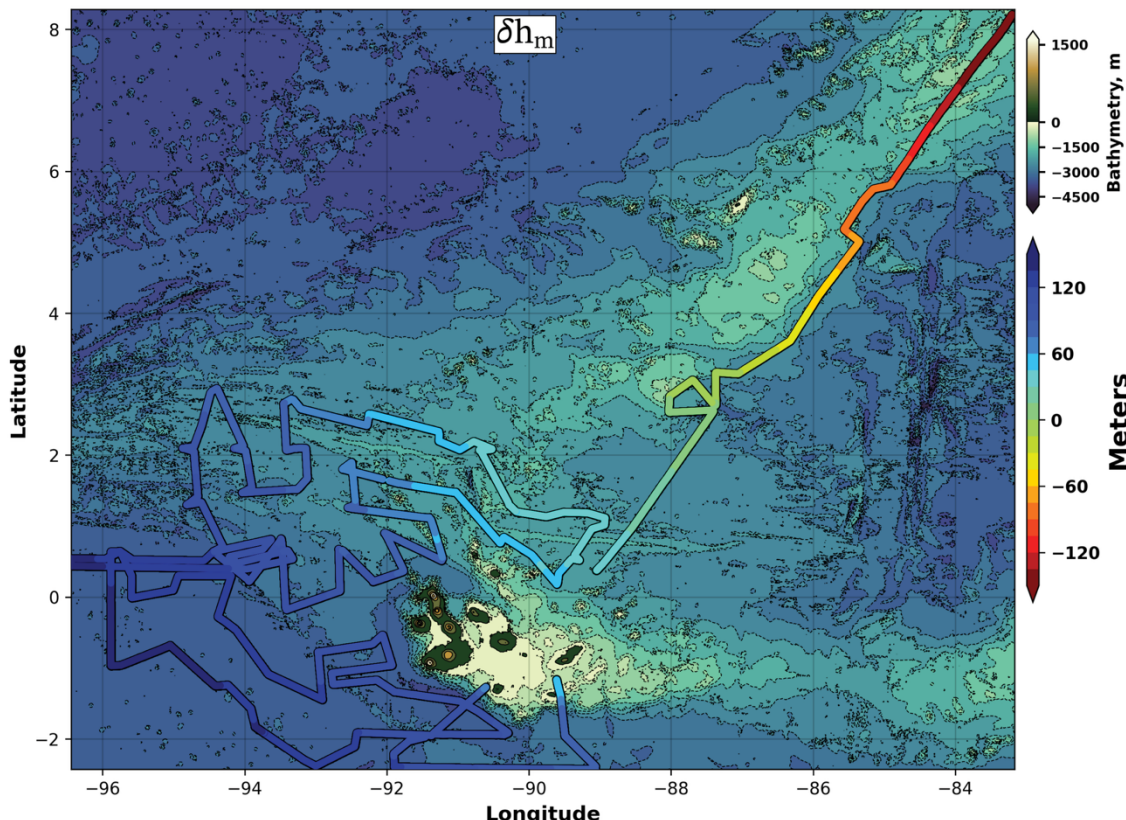


Figure 4. Perturbations to the Moho depth when using the Bouguer slab equation to estimate depth from free-air surface anomaly using a reference geoid instead of a reference ellipsoid. This is essentially just the negative geoid height anomaly times the free-air gradient (0.3086 mGal/m). The map background is bathymetry.

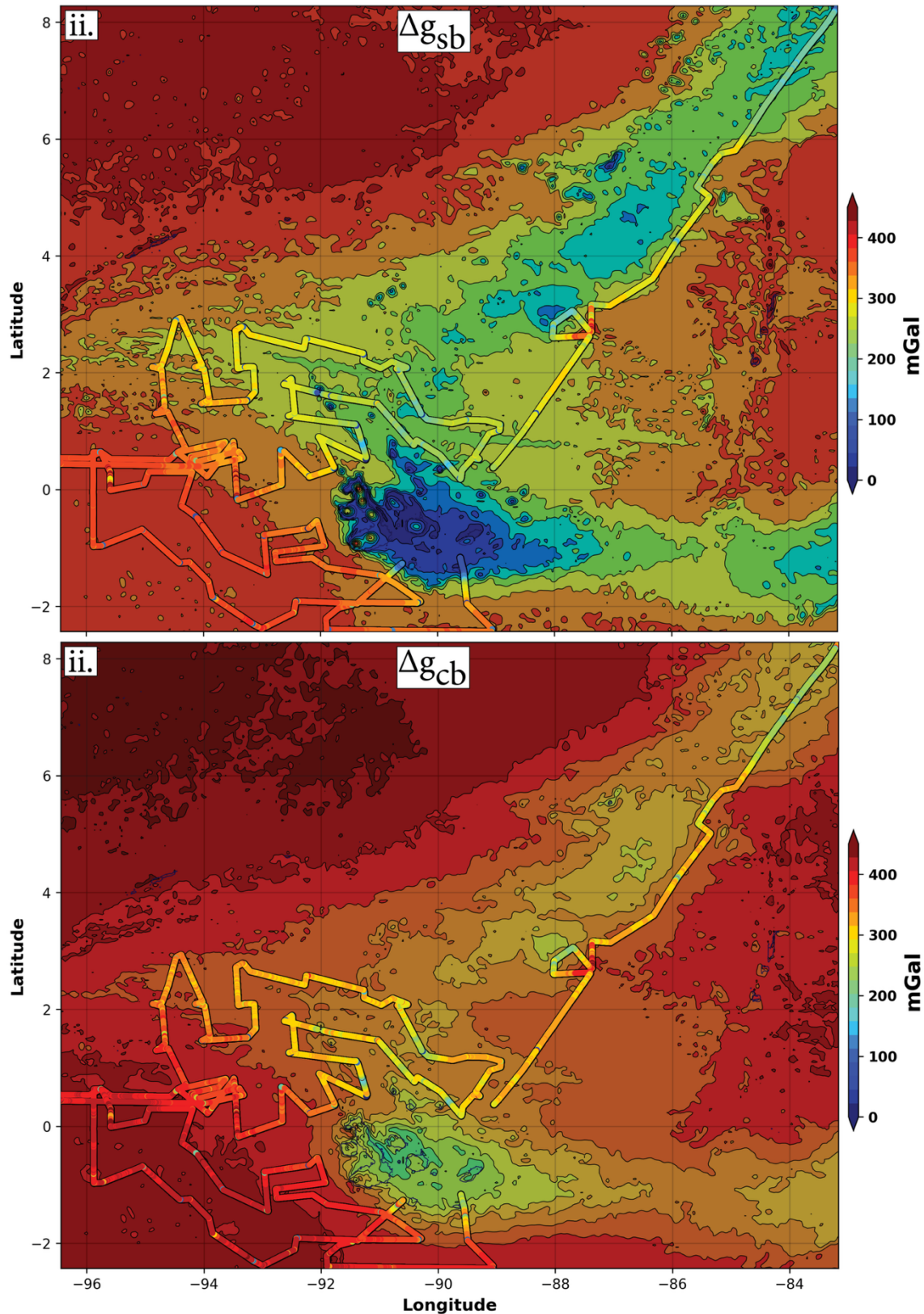


Figure 5. Simple (i.) and complete (ii.) bouguer anomalies (for $\rho=2,670 \text{ kg/m}^3$) from the Iguaña recovery cruise data with the WGM2012 complete bouguer anomaly in the background for comparison. In the simple Bouguer anomaly (i.), the warmer (reds) colors are generally related to a relatively thicker lithosphere than the colder (blues). In the complete Bouguer anomaly (ii.), colder-warm transitions represents finer lateral variations in increasing density structure going out from the Cocos ridge or Galapagos hotspot to the open ocean.

WGM2012. The simple bouguer anomaly shows positive anomalies where mass deficits exceeds the crust density used in eq. 4 ($2,670 \text{ kg/m}^3$) such as those shown in the open ocean far from the ridge and islands. The opposite is shown where the negative anomalies under-predict the mass deficits (relative to $2,670 \text{ kg/m}^3$) such as those shown along the ridge and Galápagos hotspot. After correcting for the lack of terrain considered in the simple bouguer anomaly (eq. 5), the complete bouguer shows lower amplitude anomalies associated with lateral variations in crustal composition. The lowest values in the complete Bouguer anomalies are shown directly beneath the active volcanoes on the islands of Fernandina and Isabela.

Discussion

The simple and complete Bouguer anomalies reveal broad trends consistent with westward-thickening lithosphere, overprinted by shorter-wavelength negative anomalies indicative of localized mass deficits likely linked to active mantle processes beneath the western Galápagos Spreading Center, the Cocos Ridge, and the Galápagos plume. Interpreted under the assumption of constant crustal thickness, these anomalies would suggest variations in the thickness or density of the mantle lithosphere. However, due to the inherent non-uniqueness of gravity data with respect to vertical density structure, the negative anomalies could reflect either a locally thinner lithosphere, active mantle upwelling, or a combination of both. While free-air disturbances show broad agreement with the isostatically compensated anomalies in WGM2012, the use of an Airy–Heiskanen isostasy model (Heiskanen and Moritz, 1967; Watts, 2001) is problematic when applied to oceanic lithosphere. Airy-type models allow compensation via crustal thickness variations, which contradict the relatively uniform thickness of oceanic crust globally. As shown in prior studies(Boschi et al., 2010; Bagherbandi and Sjöberg, 2012; Laske et al., 2013; Szwilus et al., 2016; Kirby, 2018), a Pratt-style or flexural isostasy model is more appropriate for such regions, where lateral density variations or elastic support better explain observed gravity patterns. The Airy approach, when applied naively to deep oceanic seafloor, can even predict physically implausible Moho depths that lie above the seafloor (Szwilus et al., 2016). Nonetheless, the observed similarity between cruise-derived free-air disturbances and the WGM2012 isostatic anomaly likely reflects real structural variations within the uppermost ~30 km that are not exclusively governed by the Airy isostatic model used in the reference dataset. Alternatively, these similarities may partly reflect deeper variations within the mantle lithosphere, although the predominantly short-wavelength and heterogeneous character of the anomalies favors a shallow origin.

Conclusions

Here, we have presented the methodology and results for computing the free-air anomaly, simple Bouguer anomaly, and complete Bouguer anomaly using gravity data collected during the Iguana recovery cruise and compare these results with the corresponding models from WGM2012. We further define and evaluate the free-air gravity disturbance, using it as a complementary diagnostic of subsurface mass anomalies independent of ellipsoidal reference bias. Comparison with the WGM2012 isostatically compensated Bouguer anomaly reveals that prominent structures in both the free-air

anomaly and the free-air disturbance are not adequately accounted for by an Airy-Heiskanen style isostatic compensation, particularly in regions influenced by dynamic mantle processes.

The simple Bouguer anomaly highlights broad gravity lows associated with crustal and lithospheric thinning, while the complete Bouguer anomaly resolves shorter-wavelength features tied to local bathymetric and density variations. In both cases, strong negative anomalies coincide with the Galápagos plume region, the western Galápagos Spreading Center, and parts of the Cocos Plate, consistent with an interpretation of a relatively thin mantle lithosphere and/or ongoing mantle upwelling. These findings suggest that flexural or dynamic support mechanisms, rather than local crustal root compensation alone, dominate the observed gravity field in this region. Together, these models help distinguish between topography supported by shallow density contrasts and that maintained by deeper geodynamic processes, underscoring the limitations of static isostatic assumptions in tectonically and volcanically active oceanic regions like the Galápagos.

References

- Bagherbandi, M., and L. E. Sjöberg, 2012, Non-isostatic effects on crustal thickness: A study using CRUST2. 0 in Fennoscandia: Physics of the Earth and Planetary Interiors, **200**, 37–44.
- Balmino, G., and S. Bonvalot, 2016, Gravity Anomalies, in E. Grafarend, ed., Encyclopedia of Geodesy, Springer International Publishing, 1–9.
- Barrera-Lopez, C. V., W. D. Mooney, and M. K. Kaban, 2022, Regional Geophysics of the Caribbean and Northern South America: Implications for Tectonics: Geochemistry, Geophysics, Geosystems, **23**, e2021GC010112.
- Boschi, L., C. Faccenna, and T. Becker, 2010, Mantle structure and dynamic topography in the Mediterranean Basin: Geophysical Research Letters, **37**.
- Chapman, M. E., and J. H. Bodine, 1979, Considerations of the indirect effect in marine gravity modeling: Journal of Geophysical Research: Solid Earth, **84**, 3889–3892.
- Cronin, V. S., 1992, Types and kinematic stability of triple junctions: Tectonophysics, **207**, 287–301.
- DeMets, C., R. G. Gordon, D. Argus, and S. Stein, 1990, Current plate motions: Geophysical Journal International, **101**, 425–478.
- Eötvös, R. v, 1922, Beitrage zum gesetze der proportionalitat von tragheit und gravitat: Annales de Physique, **68**, 11–66.
- Hackney, R. I., and W. E. Featherstone, 2003, Geodetic versus geophysical perspectives of the ‘gravity anomaly’: Geophysical Journal International, **154**, 35–43.
- Harpp, K. S., and D. J. Geist, 2018, The Evolution of Galápagos Volcanoes: An Alternative Perspective: Frontiers in Earth Science, **6**, 50.
- Heiskanen, W. A., and H. Moritz, 1967, Physical geodesy: Bulletin Géodésique (1946-1975), **86**, 491–492.
- Hooft, E., D. Toomey, and G. Apuzen-Ito, 2023, An open access experiment to seismically image galapagos plume-ridge interaction: .
- Kirby, J. F., 2018, On the pitfalls of Airy isostasy and the isostatic gravity anomaly in general: Geophysical Journal International.
- Laske, G., G. Masters, Z. Ma, and M. Pasyanos, 2013, Update on CRUST1. 0—A 1-degree global model of Earth’s crust: Geophysical Research Abstracts, **15**, 2658.
- Lemoine, F. G., S. C. Kenyon, J. K. Factor, R. G. Trimmer, N. K. Pavlis, D. S. Chinn, C. M. Cox, S. M. Klosko, S. B. Luthcke, M. H. Torrence, and others, 1998, The Development of the Joint NASA GSFC and the National Imagery and Mapping Agency (NIMA) Geopotential Model EGM96:
- Oldenburg, D. W., 1974, The inversion and interpretation of gravity anomalies: Geophysics, **39**, 526–536.
- Parker, R. L., 1973, The Rapid Calculation of Potential Anomalies: Geophysical Journal International, **31**, 447–455.
- Sinton, C. W., D. M. Christie, and R. A. Duncan, 1996, Geochronology of Galápagos seamounts: Journal of Geophysical Research: Solid Earth, **101**, 13689–13700.
- Szwilus, W., J. Ebbing, and N. Holzrichter, 2016, Importance of far-field topographic and isostatic corrections for regional density modelling: Geophysical Journal International, **207**, 274–287.
- Watts, A. B., 2001, Isostasy and Flexure of the Lithosphere: Cambridge University Press.

Zheng, T., J. Lin, H. Schouten, D. K. Smith, E. Klein, and R. Parnell-Turner, 2023, Gravity Anomalies and Implications for Shallow Mantle Processes of the Western Cocos-Nazca Spreading Center: Geophysical Research Letters, **50**, e2022GL102133.